The effect of non-Newtonian behavior on contact formation in an external gear pump

Journal of Non-Newtonian Fluid Mechanics 306 (2022) 104818

Contents lists available at ScienceDirect

Journal of Non-Newtonian Fluid Mechanics

journal homepage: www.elsevier.com/locate/jnnfm

The effect of non-Newtonian behavior on contact formation in an external gear pump

Vincent G. de Bie [a,b], Martien A. Hulsen [a], Patrick D. Anderson [a,*]

[a] Department of Mechanical Engineering, Eindhoven University of Technology, P.O. Box 513, 5600 MB Eindhoven, The Netherlands
[b] VMI Holland B.V., Gelriaweg 16, 8161 RK Epe, The Netherlands

ARTICLE INFO

Keywords:
Numerical simulations
Finite element method
External gear pump
Contact
Shear thinning
Compressible
Pressure-dependent viscosity

ABSTRACT

In an extrusion process, an external gear pump can be used to control the flow rate of the system. When extruding polymers, the viscosity is quite high, resulting in negligible inertia and thus laminar flow. The external gear pump contains two gears, one driven by a motor and one driven by means of contact with the other gear. In our previous work, the flow of a viscous fluid through an external gear pump was studied using the finite element method. Local mesh refinement was applied based on the respective distance between boundaries. Furthermore, the rotation of both gears was imposed. In this work, the rotation of one gear is imposed, whereas the other gear is freely rotating. However, the minimum distance between the gears is limited to a minimum value. When this value is reached, contact is assumed and also the rotation of second gear is imposed. A reversion of the torque on this gear results in a release of contact. In this manner, a quasi driver/driven situation is created in the numerical simulations. It is observed that contact is released periodically, and thus cannot be assumed present continuously, as is often prescribed. Non-Newtonian material properties, such as shear thinning and the pressure dependence of the density or the viscosity, alter how long contact is released during a tooth rotation.

1. Introduction

The external gear pump is a positive displacement pump and is used to transport all kinds of fluids. In this pump the rotation is imposed on the, so-called, driver gear. The rotation of the other gear, i.e. the driven gear, is imposed by means of contact with the driver gear. The fluid is transported from the suction side to the pressure side of the pump, that is, from the inflow channel to the outflow channel. Separation of the gears on the suction side, creates a vacuum which results in suction of the fluid. This fluid is trapped in the inter-teeth volumes and transported to the pressure side of the pump. Here, the fluid is pushed out of the pump due to the meshing of the gears.

Different studies focused on numerically predicting the performance of an external gear pump. During operation the gears form contact, where the contact point displaces over the contact line and jumps from one tooth to the next. Simulating such a dynamic contact point is quite complex using numerical methods. Many approaches are tried to approximate a contact point, such as a minimum distance of a couple of micrometers between the gears [1–4] or an increasing viscosity at the point of contact [5,6]. Nonetheless, in all these studies the rotation of both gears is imposed. To the authors knowledge, it is uncertain if contact does persist in practice during the whole rotation. Therefore, solving the rotation speed of the driven gear as an additional unknown in the numerical simulations can give extra information about the formation and release of contact during the rotation of the gears.

In previous studies of the authors [4,7], finite element simulations of an external gear pump are developed with the rotation of both gears imposed. A fluctuation of the output, i.e. flow rate of the pump and pressure difference over the pump, is perceived with a frequency that is related to the number of teeth of a gear. A fluctuation in the output of an extrusion process is undesired, since this results in inconsistent dimensions of the extrudate. Fluctuating output is especially unfavorable when one attempts to design a die shape at certain processing conditions to optimize the extrudate dimensions for rheologically complex materials [8–10]. It is observed that the shape of this output fluctuation is strongly dependent on the chosen minimum gap between the gears. This is especially the case for strongly shear-thinning fluids. In practice, it is presumed that a contact point forms between the gears. This would prevent that fluid can flow in-between the gears from the pressure side to the suction side. Often, it is attempted in simulations to limit this flow by using a minimum distance between the gears of a couple of micrometers.

* Corresponding author.
E-mail address: p.d.anderson@tue.nl (P.D. Anderson).

https://doi.org/10.1016/j.jnnfm.2022.104818
Received 4 March 2022; Received in revised form 25 April 2022; Accepted 29 April 2022
Available online 21 May 2022

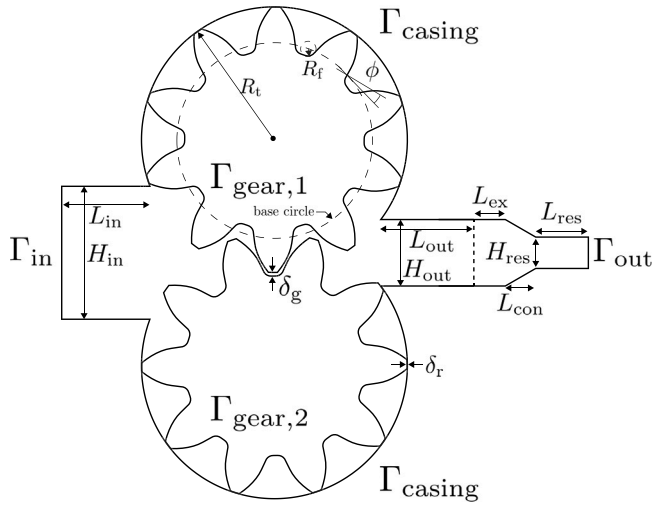

Fig. 1. Schematic representation of the dimensions of the external gear pump. See Table 1 for details on definition symbols and values used.

In this study, the two-dimensional flow of viscous fluids through an external gear pump is again numerically studied using the finite element method (FEM). However, now solely the rotation of one gear is imposed, which results in the introduction of the concept of the minimum gap size. The narrow gaps in the pump are captured using local mesh refinement. The aim of this work is to understand how non-Newtonian fluid properties influence the formation and release of contact. Hence, the effect of incorporating shear thinning or a pressure dependence of the density and viscosity on contact formation is studied. The step-by-step introduction of these phenomena reveals if one of these factors could for example drive the formation of a lubrication layer between the gears of the external gear pump.

2. Problem definition and governing equations

The flow of viscous fluids through an external gear pump is considered. The two-dimensional representation of the external gear pump of our previous study [4] is used, as is shown in Fig. 1. The external gear pump consists of a straight inflow channel, two gears with N_{t} symmetric teeth surrounded by a circular casing, and a straight outflow channel. A resistance channel is added behind the exit of the pump (dashed line in Fig. 1) to mimic the resistance that is present due to everything after the gear pump. For the shape of the resistance a contraction flow is chosen, since the start-up time in a simulation of a compressible fluid strongly depends on the length of the flow problem. With a contraction flow, the length of the flow problem can be kept approximately equal. The resistance of the contraction flow is changed by varying the value of the height H_{res}, which is the height of the channel after the contraction. The dimensions of the external gear pump are given in Table 1.

2.1. Governing equations

The mass and momentum balance are used to describe the flow of the fluid. The balance equations for an incompressible fluid, negligible inertia and no body forces are given by:

$$\nabla \cdot \boldsymbol{u} = 0 \qquad \text{in } \Omega, \tag{1}$$

$$-\nabla p + \nabla \cdot \boldsymbol{\tau} = \boldsymbol{0} \qquad \text{in } \Omega, \tag{2}$$

where $\boldsymbol{u}$ is the velocity vector, p the pressure, and $\boldsymbol{\tau}$ the extra stress tensor. For the extra stress tensor, a generalized Newtonian model is used with a viscosity depending on shear rate and pressure:

$$\boldsymbol{\tau} = 2\eta(\dot{\gamma}, p)\boldsymbol{D}, \tag{3}$$

Table 1
The dimensions of the external gear pump.

Dimension	Symbol	Value	Unit
Height inlet	H_{in}	50	mm
Length inlet	L_{in}	25	mm
Clearance gear–gear	δ_{g}	0.5	mm
Clearance gear–casing	δ_{r}	1.0	mm
Height outlet	H_{out}	25	mm
Length outlet	L_{out}	25	mm
Length before contraction	L_{ex}	5	mm
Length contraction	L_{con}	20	mm
Length after contraction	L_{res}	25	mm
Number of teeth	N_{t}	10	
Tip radius	R_{t}	50	mm
Pressure angle	ϕ	25	°
Fillet radius	R_{f}	5.0	mm

where η is the viscosity function, and $\dot{\gamma} = \sqrt{2\boldsymbol{D} : \boldsymbol{D}}$ the magnitude of the rate-of-deformation tensor $\boldsymbol{D} = (\nabla \boldsymbol{u} + (\nabla \boldsymbol{u})^T)/2$. An example of high-viscosity fluids are polymers, which typically display shear-thinning behavior and have a pressure-dependent viscosity [11,12]. The viscosity function therefore consists of the Carreau model with a pressure-dependent zero-shear viscosity and a viscosity at infinite shear rate equal to zero:

$$\eta = \frac{\eta_0(p)}{\left[1 + (\lambda\dot{\gamma})^2\right]^{\frac{1-n}{2}}}, \tag{4}$$

where η_0 is the zero-shear viscosity, n the power-law index, and λ a characteristic time. The value of λ is equal to 10 s in all simulations performed in this study, since then the shear rates $\dot{\gamma}$ observed in-between the gears and between the gears and the casing are well within the shear-thinning region. An exponential relation is used for the pressure dependence of the zero-shear viscosity:

$$\eta_0 = \frac{\eta_{0,\text{ref}}\eta_{0,\infty}}{\eta_{0,\text{ref}} + (\eta_{0,\infty} - \eta_{0,\text{ref}})\exp(-\beta(p - p_{\text{ref}}))}, \tag{5}$$

where $\eta_{0,\text{ref}}$ is the viscosity at zero shear rate and reference pressure p_{ref}, $\eta_{0,\infty}$ the viscosity at zero shear rate and infinite pressure, and β the pressure coefficient. In this work, a value of zero is used for the reference pressure p_{ref}. Fig. 2a shows the dependence of the viscosity on pressure at a shear rate of zero for a strongly shear-thinning fluid ($n = 0.2$) with different values of the pressure coefficient β. For the pressure dependence, a plateau viscosity is used to limit the rise in viscosity for extreme values of the pressure.

In this research, different values for the power-law index n are used. For $n = 1$, the viscosity is independent of the shear rate, whereas a power-law index below one results in shear-thinning behavior. Different values of the power-law index are compared by matching their viscosity at the effective shear rate, which is defined as:

$$\dot{\gamma}_{\text{eff}} = \frac{\omega_1 R_{\text{t}}}{\delta_{\text{r}}}, \tag{6}$$

where ω_1 is the rotation speed of the upper gear, R_{t} the tip radius of the gears and δ_{r} the clearance between the gears and the casing. Fig. 2b displays the dependence of the viscosity on the shear rate for various values of the power-law index n at the reference pressure. The gray dashed line in the figure denotes the effective shear rate for $\omega_1 = 1$ rad/s, the rotation speed used for all simulations in this work.

If we study a compressible fluid, solely the mass balance equation changes, since the fluid volume is not constant. When assuming the following relation

$$p = p_{\text{ref}} - K\ln(J), \tag{7}$$

where J is the relative volume as compared to the value at reference pressure p_{ref}, then the mass balance for a compressible fluid becomes:

$$\frac{1}{K}\left(\frac{\partial p}{\partial t} + \boldsymbol{u} \cdot \nabla p\right) + \nabla \cdot \boldsymbol{u} = 0 \qquad \text{in } \Omega, \tag{8}$$

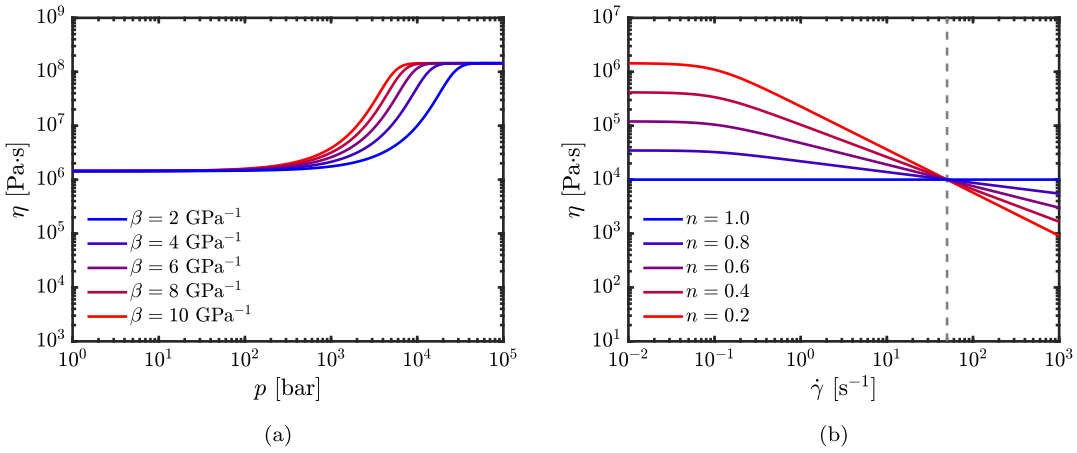

Fig. 2. The effect of varying coefficients in the viscosity function for a pressure-dependent shear-thinning fluid using $\lambda = 10$ s, $\eta_{0,\infty} = 10^2\eta_{0,\text{ref}}$, and $\eta(\dot{\gamma}_{\text{eff}}, p_{\text{ref}}) = 10^4$ Pa s: (a) varying pressure coefficient β at $\dot{\gamma} = 0$ s^{-1} for $n = 0.2$, and (b) varying power-law index n with $p = p_{\text{ref}}$.

where K is the bulk modulus and t is the time. Since solely pressure gradients are present in Eq. (8), the reference pressure does not need to be defined for solving the mass balance equation. However, the absolute value of the reference pressure is needed for the pressure dependence of the viscosity.

2.2. Initial and boundary conditions

To fill the external gear pump, often an extruder is placed in front of the pump. Complete filling is assured by letting the extruder generate a certain entry pressure p_{in} at the inlet (Γ_{in}). Along with that, the flow at the inlet is assumed to be fully developed. This results in the following boundary conditions:

$$p = p_{\text{in}} \qquad \text{on } \Gamma_{\text{in}}, \tag{9}$$

$$u_y = 0 \qquad \text{on } \Gamma_{\text{in}}. \tag{10}$$

An entry pressure of 10 bar is used in all simulations in this work. It is assumed that there is no slip, and thus the velocity at the casing (Γ_{casing}) is:

$$\boldsymbol{u} = \boldsymbol{0} \qquad \text{on } \Gamma_{\text{casing}}. \tag{11}$$

The rotation of the upper gear ($\Gamma_{\text{gear},1}$) is imposed. Since no slip is assumed, the fluid at the gear boundary has the same rotation speed as the gear:

$$\boldsymbol{u} = \omega_1 r \boldsymbol{e}_\theta \qquad \text{on } \Gamma_{\text{gear},1}, \tag{12}$$

where r is the distance to the gear center and $\boldsymbol{e}_\theta$ the tangential to a circle with the origin in the gear center and radius r. The lower gear ($\Gamma_{\text{gear},2}$) is assumed to be freely rotating, and thus:

$$\boldsymbol{u} = -\omega_2 r \boldsymbol{e}_\theta \qquad \text{on } \Gamma_{\text{gear},2}, \tag{13}$$

where the rotation speed ω_2 is such that the torque balance for the gear is fulfilled. The minus sign in Eq. (13) ensures that ω_2 is a positive number, since the rotation direction of the lower gear is counterclockwise. Thus, the lower gear is freely rotating, i.e. torque free

$$\int_{\Gamma_{\text{gear},2}} r\boldsymbol{e}_\theta \cdot (\boldsymbol{\sigma} \cdot \boldsymbol{n})\, ds = 0, \tag{14}$$

where $\boldsymbol{\sigma} = -p\boldsymbol{I} + \boldsymbol{\tau}$ is the Cauchy stress tensor and $\boldsymbol{n}$ the outwardly directed normal vector. A fully developed flow with zero horizontal traction is assumed at the outlet of the resistance channel (Γ_{out}):

$$t_x = 0 \qquad \text{on } \Gamma_{\text{out}}, \tag{15}$$

$$u_y = 0 \qquad \text{on } \Gamma_{\text{out}}, \tag{16}$$

where $\boldsymbol{t} = \boldsymbol{\sigma} \cdot \boldsymbol{n}$ is the traction vector. Initially, the angle difference between the gears $\Gamma_{\text{gear},1}$ and $\Gamma_{\text{gear},2}$ is π/N_{t}, which is half a gear tooth. When considering a compressible fluid, an initial pressure distribution is required. The solution for the incompressible fluid is used as the initial condition for the pressure.

3. Numerical method

The governing equations are solved using the finite element method (FEM). The simulations are developed in an in-house research package, called TFEM. In this section, first the weak form is derived. Thereafter, the discretization of space and time is explained with an emphasis on local mesh refinement. Also the concept of minimum gap size is introduced in this part. Finally, the iteration schemes are discussed.

3.1. Weak form

The boundary condition for the freely rotating gear is implemented using a constraint. This is introduced using the Lagrange multiplier λ, which imposes $\boldsymbol{u} = \omega_2 r\boldsymbol{e}_\theta$ in each point of the boundary with ω_2 an unknown constant. The weak form of the mass and momentum balance including the freely rotating gear for an incompressible fluid is then written as: Find $\boldsymbol{u}$, p, ω_2, λ such that:

$$(q, \nabla \cdot \boldsymbol{u}) = 0 \qquad \text{for all } q, \tag{17}$$

$$\left((\nabla \boldsymbol{v})^T, \boldsymbol{\tau}\right) - (\nabla \cdot \boldsymbol{v}, p) + \langle \boldsymbol{v} - \chi r\boldsymbol{e}_\theta, \lambda\rangle_{\Gamma_{\text{gear},2}} = \langle \boldsymbol{v}, \boldsymbol{t}\rangle_\Gamma \qquad \text{for all } \boldsymbol{v}, \tag{18}$$

$$\langle \boldsymbol{\mu}, \boldsymbol{u} - \omega_2 r\boldsymbol{e}_\theta\rangle_{\Gamma_{\text{gear},2}} = 0 \qquad \text{for all } \boldsymbol{\mu}, \tag{19}$$

for all admissible test functions q, $\boldsymbol{v}$, χ, and $\boldsymbol{\mu}$. In the weak forms, $(\cdot,\cdot)$ is the L_2 inner product on domain Ω, and $\langle\cdot,\cdot\rangle_\Gamma$ the L_2 inner product on boundary Γ. The constitutive model for the extra stress tensor $\boldsymbol{\tau}$ is given by Eq. (3). Note, that ω_2, and the corresponding χ, are single values for gear 2, whereas λ (and $\boldsymbol{\mu}$) are function fields on the boundary $\Gamma_{\text{gear},2}$. For a compressible fluid, Eq. (17) changes to:

$$\left(q, \frac{1}{K}\frac{\partial p}{\partial t}\right) + \left(q, \frac{1}{K}\boldsymbol{u} \cdot \nabla p\right) + (q, \nabla \cdot \boldsymbol{u}) = 0 \qquad \text{for all } q. \tag{20}$$

3.2. Discretization

The problem is discretizated using the finite element method. Discretization of space and time is performed. The time discretization for the incompressible case mainly influences the correctness of the rotation of the freely-rotating gear over time. The rotation angle of this gear is updated by

$$\theta_2(t + \Delta t) = \theta_2(t) + \omega_2(t)\Delta t, \tag{21}$$

for the first time step and when a switch in boundary conditions is applied. This switch means that we go from a state in which one gear has an imposed rotation and one is freely rotating, to a state with the rotation of both gears imposed, or vice versa. This is further explained in Section 3.2.2. For the other time steps, a second-order Adams–Bashforth scheme is used

$$\theta_2(t+\Delta t) = \theta_2(t) + \left(\tfrac{3}{2}\omega_2(t) - \tfrac{1}{2}\omega_2(t-\Delta t)\right)\Delta t. \tag{22}$$

For the compressible case, a first-order semi-implicit Euler time integration scheme is applied for the mass balance equation for the first time step and a second-order semi-implicit backward differencing scheme for all subsequent time steps.

For spatial discretization, triangular isoparametric elements are used with quadratic interpolation (P_2) of the velocity and linear interpolation (P_1) of the pressure (Taylor–Hood). For λ and $\boldsymbol{\mu}$, the sum is used over the nodes on $\Gamma_{\text{gear},2}$ where the velocity degrees of freedom are defined, and thus:

$$\langle \boldsymbol{a}, \boldsymbol{b} \rangle = \sum_{k=1}^{n_n} \boldsymbol{a}_k \cdot \boldsymbol{b}_k, \tag{23}$$

where $\boldsymbol{a}$ and $\boldsymbol{b}$ are vectors, and n_n is the number of nodes on $\Gamma_{\text{gear},2}$. The domain Ω is discretized using a meshing procedure based on the work of Mitrias et al. [13]. The procedures for mesh generation and mesh movement are similar as in our previous work [4]. A summary is given in the following subsection. A convergence study for the time and spatial discretization is performed in Section 4.1.

3.2.1. Meshing procedure

Due to the extreme differences in length scales in the problem, local mesh refinement is required to limit the number of elements of the mesh. During the meshing procedure, the boundaries of a coarse mesh are refined based on the respective distance between boundaries. In short, a certain number of elements between boundaries is assured by locally refining the boundaries. With the help of these boundaries, a Poisson problem is solved to obtain a field that displays the distribution of the element size. A locally refined mesh is then generated using the refined boundaries, the element-size field and Gmsh [14]. A resulting mesh for a situation where the minimum distance between the gears is in the order of 1 μ m is shown in Fig. 3. The information of this mesh is given in Table 2. The figure illustrates that the elements are even distributed nicely when zooming in quite significantly on the mesh between the gears. More quantitative values of the mesh quality for this mesh are given in Table 3.

The boundaries of the problem are not static, but the gears are rotating in time. Therefore, the mesh needs to be updated for every time step. Hu et al. [15] showed that a displacement field to update the nodal coordinates can be obtained by solving a Laplace equation. After updating the mesh, the mesh quality is checked. If the elements are distorted or (un)refinement is needed, remeshing is performed. In practice, a new mesh is generated numerous times during a simulation, i.e. every 5–30 time steps.

When remeshing is performed in a simulation of a compressible fluid, weak projections of the mesh coordinates and the solutions of the previous time steps are applied. The mesh coordinates are projected in order to obtain the mesh velocity $\boldsymbol{u}_m$. This velocity is used in the arbitrary Lagrange Euler (ALE) formulation [15], which is needed because we have a moving grid. The material derivative is then rewritten as

$$\frac{D()}{Dt} = \frac{\partial()}{\partial t}\Big|_{\boldsymbol{x}_m} + (\boldsymbol{u} - \boldsymbol{u}_m)\cdot(), \tag{24}$$

where the partial derivative with respect to time is computed at constant mesh coordinate $\boldsymbol{x}_m$.

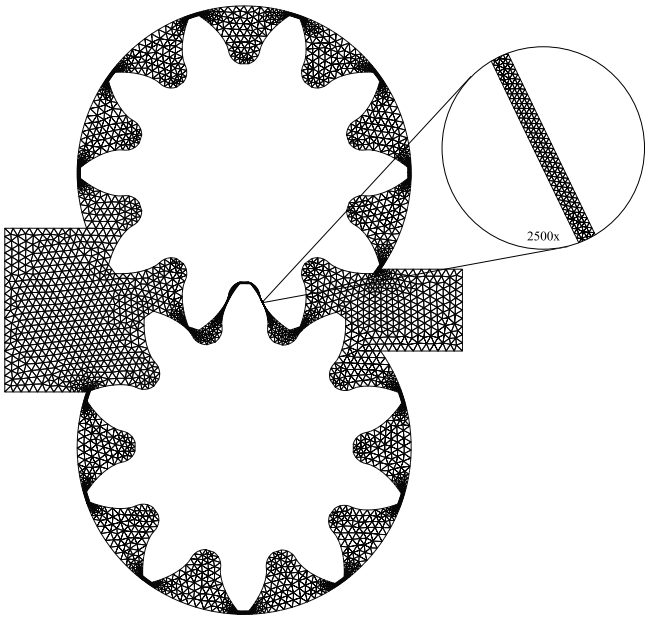

Fig. 3. Finite element mesh of the external gear pump with local mesh refinements based on the respective distance in-between boundaries with a zoom on the mesh between the gears.

Table 2
Mesh information for a mesh of the external gear pump with the minimum distance between the gears in the order of 1 μm.

Maximum element size	2.5 mm
Minimum number of elements between boundaries	2
Number of nodes	35 001
Number of elements	15 652
Number of degrees of freedom	79 677

Table 3
Mesh quality [14,16] of a mesh of the external gear pump with the minimum distance between the gears in the order of 1 μm.

Quality parameter	Average	Worst
Inscribed radius/circumscribed radius	0.7909	0.6153
min(Jacobian)/max(Jacobian)	0.998	0.328
Inverse error on the gradient of FE solution	0.989	0.805
Inverse condition number	0.974	0.698

3.2.2. Minimum gap size

The rotation of the upper gear is imposed, but the lower gear is freely rotating. Hence, the minimum distance between the gears can become very small, resulting in extremely small elements to capture the interaction between the gears. In our approach, this minimum distance is limited by a distance $d_{\min}$. When this distance is reached, contact is assumed and thus the rotation speed of both gears is equal. This is done by imposing the rotation of both gears. The lower gear is then no longer rotating freely in the fluid, and thus the fluid now exerts a torque on the gear. When this torque switches sign, a separation of the lower and the upper gear is desired. Therefore, contact is released and the rotation speed of the lower gear is again obtained using the freely-rotating constraint. The influence of the minimum gap size $d_{\min}$ is studied in Section 4.2.

3.3. Iterations

The equations for the flow of the pressure-dependent shear-thinning fluid are nonlinear in the velocity and the pressure. Therefore, the following iteration schemes to converge towards the solution are presented. The Picard iteration scheme for an incompressible fluid is

defined as: Find $\boldsymbol{u}^{(j+1)}$, $p^{(j+1)}$, $\lambda^{(j+1)}$ and $\omega_2^{(j+1)}$ such that:

$$\left(q, \nabla \cdot \boldsymbol{u}^{(j+1)}\right) = 0 \qquad \text{for all } q, \tag{25}$$

$$\left((\nabla \boldsymbol{v})^T, 2\eta_j \boldsymbol{D}_{j+1}\right) - \left(\nabla \cdot \boldsymbol{v}, p^{(j+1)}\right) + \left\langle \boldsymbol{v} - \chi r \boldsymbol{e}_\theta, \lambda^{(j+1)} \right\rangle_{\Gamma_{\text{gear},2}} = \langle \boldsymbol{v}, \boldsymbol{t}_\text{N} \rangle_{\Gamma_\text{N}} \qquad \text{for all } \boldsymbol{v}, \tag{26}$$

$$\left\langle \boldsymbol{\mu}, \boldsymbol{u}^{(j+1)} - \omega_2^{(j+1)} r \boldsymbol{e}_\theta \right\rangle_{\Gamma_{\text{gear},2}} = 0 \qquad \text{for all } \boldsymbol{\mu}, \tag{27}$$

with $j = 0, 1, \ldots$ and initial guesses $\boldsymbol{u}^{(0)}$ and $p^{(0)}$. In the equations above some abbreviations are used: $\eta_j = \eta(\dot{\gamma}(\boldsymbol{u}^{(j)}), p^{(j)})$, and $\boldsymbol{D}_{j+1} = \boldsymbol{D}(\boldsymbol{u}^{(j+1)})$. The rate of convergence of the Picard iteration scheme is rather low [17], and thus also the Newton–Raphson iteration scheme is applied. Instead of solving for the values of the velocity and pressure at the next iteration, this iteration scheme makes use of differences:

$$\Delta \boldsymbol{u} = \boldsymbol{u}^{(j+1)} - \boldsymbol{u}^{(j)}, \tag{28}$$

$$\Delta p = p^{(j+1)} - p^{(j)}. \tag{29}$$

The Newton–Raphson iteration scheme is defined as: Find $\Delta \boldsymbol{u}$, Δp, $\lambda^{(j+1)}$ and $\omega_2^{(j+1)}$ such that:

$$\left(q, \nabla \cdot \Delta \boldsymbol{u}\right) = -\left(q, \nabla \cdot \boldsymbol{u}^{(j)}\right) \qquad \text{for all } q, \tag{30}$$

$$\left((\nabla \boldsymbol{v})^T, X\right) - \left(\nabla \cdot \boldsymbol{v}, \Delta p\right) + \left\langle \boldsymbol{v} - \chi r \boldsymbol{e}_\theta, \lambda^{(j+1)} \right\rangle_{\Gamma_{\text{gear},2}} = -\left((\nabla \boldsymbol{v})^T, 2\eta_j \boldsymbol{D}_j\right) + \left(\nabla \cdot \boldsymbol{v}, p^{(j)}\right) + \langle \boldsymbol{v}, \boldsymbol{t}_\text{N} \rangle_{\Gamma_\text{N}} \qquad \text{for all } \boldsymbol{v}, \tag{31}$$

$$\left\langle \boldsymbol{\mu}, \Delta \boldsymbol{u} - \omega_2^{(j+1)} r \boldsymbol{e}_\theta \right\rangle_{\Gamma_{\text{gear},2}} = -\left\langle \boldsymbol{\mu}, \boldsymbol{u}^{(j)} \right\rangle_{\Gamma_{\text{gear},2}} \qquad \text{for all } \boldsymbol{\mu}. \tag{32}$$

where $X = \frac{4\eta_{j,\dot{\gamma}}}{\dot{\gamma}_j} \boldsymbol{D}_j \boldsymbol{D}_j : \Delta \boldsymbol{D} + 2\eta_j \Delta \boldsymbol{D} + 2\eta_{j,p} \boldsymbol{D}_j \Delta p$. Furthermore, $\eta_{j,\dot{\gamma}} = \partial \eta / \partial \dot{\gamma}$, $\eta_{j,p} = \partial \eta / \partial p$, $\boldsymbol{D}_j = \boldsymbol{D}(\boldsymbol{u}^{(j)})$ and $\Delta \boldsymbol{D} = \boldsymbol{D}(\Delta \boldsymbol{u})$. The partial derivatives of the viscosity η are evaluated using the velocities and pressures of iteration (j): $\boldsymbol{u}^{(j)}$ and $p^{(j)}$. The respective derivatives of the viscosity are given by:

$$\frac{\eta_{j,\dot{\gamma}}}{\dot{\gamma}} = -\frac{\eta_{0,\text{ref}} \eta_{0,\infty}}{\eta_{0,\text{ref}} + (\eta_{0,\infty} - \eta_{0,\text{ref}}) \exp(-\beta(p_j - p_\text{ref}))} \frac{(1-n)\lambda^2}{(1 + (\lambda \dot{\gamma}(\boldsymbol{u}_j))^2)^{\frac{3-n}{2}}}, \tag{33}$$

$$\eta_{j,p} = \frac{\eta_{0,\text{ref}} \eta_{0,\infty} (\eta_{0,\infty} - \eta_{0,\text{ref}}) \beta \exp(-\beta(p_j - p_\text{ref}))}{(\eta_{0,\text{ref}} + (\eta_{0,\infty} - \eta_{0,\text{ref}}) \exp(-\beta(p_j - p_\text{ref})))^2} \frac{1}{(1 + (\lambda \dot{\gamma}(\boldsymbol{u}_j))^2)^{\frac{1-n}{2}}}. \tag{34}$$

Note that due to the viscosity function, starting values for velocity and pressure are needed for both iteration schemes. A Stokes solution is used as the starting values for the first time step and when projections are not applied also for the subsequent time steps. Thus, for a compressible fluid the solution of the previous time step can be taken as the starting value, resulting in faster convergence. Due to the complex flow problem, the Newton–Raphson iteration scheme has a narrow convergence window. Therefore, first a number of Picard iterations is applied before switching to Newton–Raphson. The number of Picard iterations needed to obtain convergence depends on the material behavior but is in the order of 10–50 iterations, where the total number of iterations ranges up to 200. For a strongly shear-thinning fluid, the number of iterations is for most of the time steps around 60.

When a compressible fluid is studied, time interpolation needs to be applied. Thus, for first-order time integration with a time step Δt, Eq. (25) transforms into:

$$\left(q, \frac{p^{(j+1)}(t+\Delta t)}{\Delta t}\right) + \left(q, \boldsymbol{u}^{(j)}(t+\Delta t) \cdot \nabla p^{(j+1)}(t+\Delta t)\right) + \left(q, \nabla \cdot \boldsymbol{u}^{(j+1)}(t+\Delta t)\right) = \left(q, \frac{p(t)}{\Delta t}\right) \qquad \text{for all } q, \tag{35}$$

and Eq. (30) into:

$$\left(q, \frac{\Delta p(t+\Delta t)}{\Delta t}\right) + \left(q, \boldsymbol{u}^{(j)}(t+\Delta t) \cdot \nabla \Delta p(t+\Delta t)\right) + \left(q, \Delta \boldsymbol{u}(t+\Delta t) \cdot \nabla p^{(j)}(t+\Delta t)\right) + \left(q, \nabla \cdot \Delta \boldsymbol{u}(t+\Delta t)\right) = \left(q, \frac{p(t)}{\Delta t}\right) - \left(q, \frac{p^{(j)}(t)}{\Delta t}\right) - \left(q, \boldsymbol{u}^{(j)}(t+\Delta t) \cdot \nabla p^{(j)}(t+\Delta t)\right) - \left(q, \nabla \cdot \boldsymbol{u}^{(j)}(t+\Delta t)\right) \qquad \text{for all } q. \tag{36}$$

A direct solver, i.e. the Pardiso solver integrated in the MKL library, is used on four parallel cores to solve the system of equations as outlined above.

4. Results

In this section, a mesh and time convergence study is performed to assure accurate results. Second, the influence of the minimum gap size is studied. Thereafter, the results of numerical simulations using Newtonian, shear-thinning, compressible and pressure-thickening fluids are discussed.

4.1. Mesh and time convergence

To assure an accurate simulation, a convergence study is performed. In contrast to our previous work [4], the solution is now dependent on the history due to the time dependence of the rotation speed of the freely rotating gear. Therefore, the time step cannot be freely chosen. Additionally, for the compressible case the fluid volume is dependent on time. The error in this convergence study for a certain time step or element size is defined as

$$\text{e} = \frac{\max |\omega_2(t) - \omega_{2,\text{ref}}(t)|}{\max(\omega_{2,\text{ref}}(t))}, \tag{37}$$

where subscript "ref" indicates the reference time step or element size. The convergence study is performed for the shear-thinning fluid with a power-law index of $n = 0.2$. The strong dependence of the viscosity on the shear rate combined with one of the largest rotation speeds of the freely rotating gear make this an interesting case for the convergence study. The maximum error is obtained for a time below 0.373 s, since up till this time no switch between boundary conditions is performed.

The resulting errors for a certain range of time steps are shown in Fig. 4a. The reference time step is ten times smaller than the smallest time step in the plot. A limiting factor for the time step is that it needs to be small enough in order to prevent overlapping of the gears during the whole simulation. The error definitely becomes smaller for decreasing time step. For the largest possible time step, the error is already lower as 1% and thus this amount of time steps is used in the simulations with shear-thinning fluids. The time step in these simulations is defined as $\Delta t = 2\pi/(n_\text{steps} \omega_1 N_\text{t})$, where $n_\text{steps} = 1440$. However, when including compressibility the number of time steps is increased to $n_\text{steps} = 5760$.

The spatial convergence of the simulation also needs to be assured. Solely, the number of elements between the boundaries is varied by changing the value of R_crit, because it is expected that the size of these elements is most essential. The maximum element size in domain Ω is set to $\Delta h = 2.5$ mm. For the reference case, the value of R_crit is equal to sixteen. Fig. 4b shows that the error decreases for increasing value of R_crit. It can also be seen that every value of R_crit is sufficient to get below the convergence criterion of 1%. However, our previous study [4] showed that at least two elements are needed between the boundaries for the accuracy of the output of the external gear pump. Hence, $R_\text{crit} = 2$ is used for all simulations performed in this work.

4.2. Minimum gap size

The results of the simulations are mainly presented in this work by showing the output in terms of the difference in rotation speed between the gears $\omega_2 - \omega_1$, the minimum distance between the gears Δx, the flow rate of the pump Q and the mean pressure difference over the pump $\overline{\Delta p}$. This output of the pump is presented for 1.5 s, which is approximately equal to the rotation of three gear teeth of the upper gear. The minimum distance between the gears is the minimum value of the respective distances between the nodes on the gear boundaries. The

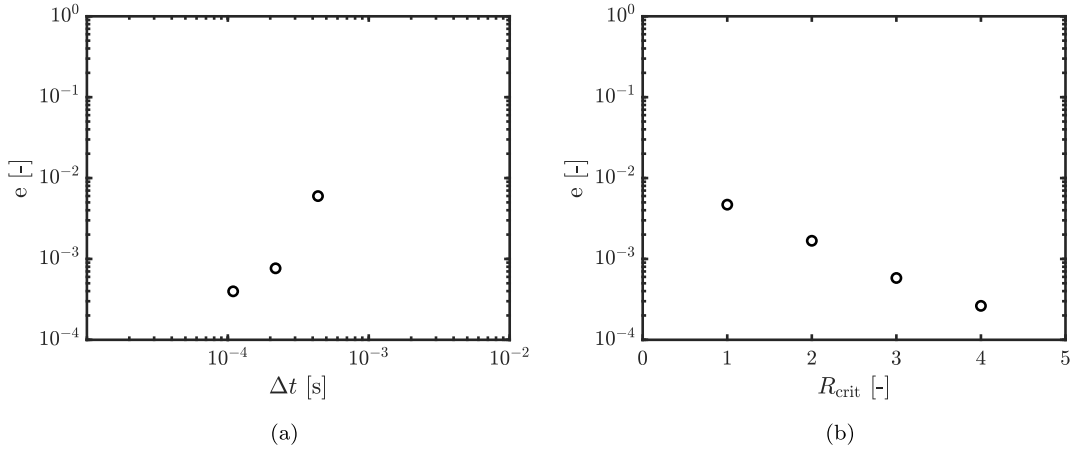

Fig. 4. The maximum relative error of the rotation speed of the freely rotating gear of the external gear pump, with $\omega_1 = 1$ rad/s and $\overline{\Delta p} \approx 100$ bar, processing a shear-thinning fluid ($n = 0.2$) with $\eta(\dot{\gamma}_{\text{ref}}) = 10^4$ Pa s, as a function of: (a) time step Δt, and (b) refinement criterion R_{crit}.

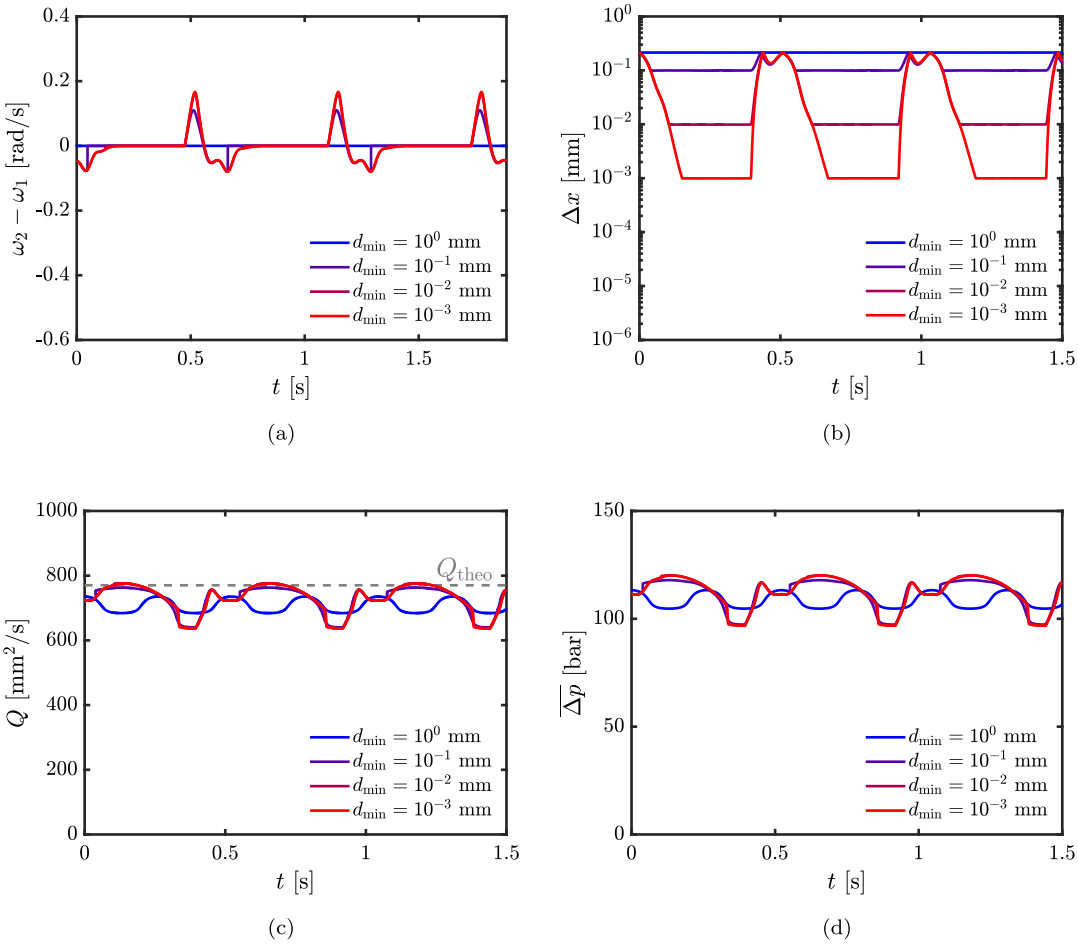

Fig. 5. The output of numerical simulations of the external gear pump, with $\omega_1 = 1$ rad/s and $\overline{\Delta p} \approx 100$ bar, processing a Newtonian fluid ($n = 1$) with $\eta_0 = 10^4$ Pa s, for varying minimum gap size: (a) rotation speed difference $\omega_2 - \omega_1$, (b) minimum distance Δx, (c) flow rate Q, and (d) mean pressure difference $\overline{\Delta p}$.

flow rate is obtained by numerical integration of the horizontal velocity over the exit of the pump, which is shown as a black dashed line in Fig. 1. In case of a compressible fluid, the flow rate is also obtained at the entry of the pump. Note that, since a 2D simulation is used, the unit of the flow rate is mm^2/s. The theoretically achievable flow rate is given by a horizontal gray dashed line in the plots of the flow rate and is obtained by subtracting the area of the gear from a circle with the tip radius, which is then multiplied by the number of rotations per second and the number of gears. The mean pressure difference over the pump is computed by:

$$\overline{\Delta p} = \frac{1}{n_{\text{p}}} \sum_{i=1}^{n_{\text{p}}} p_i - p_{\text{in}}, \tag{38}$$

where n_{p} is the number of sample points over the pump exit.

In the simulations of the external gear pump, a minimum gap size is introduced as explained in Section 3.2.2. Fig. 5 displays the effect of

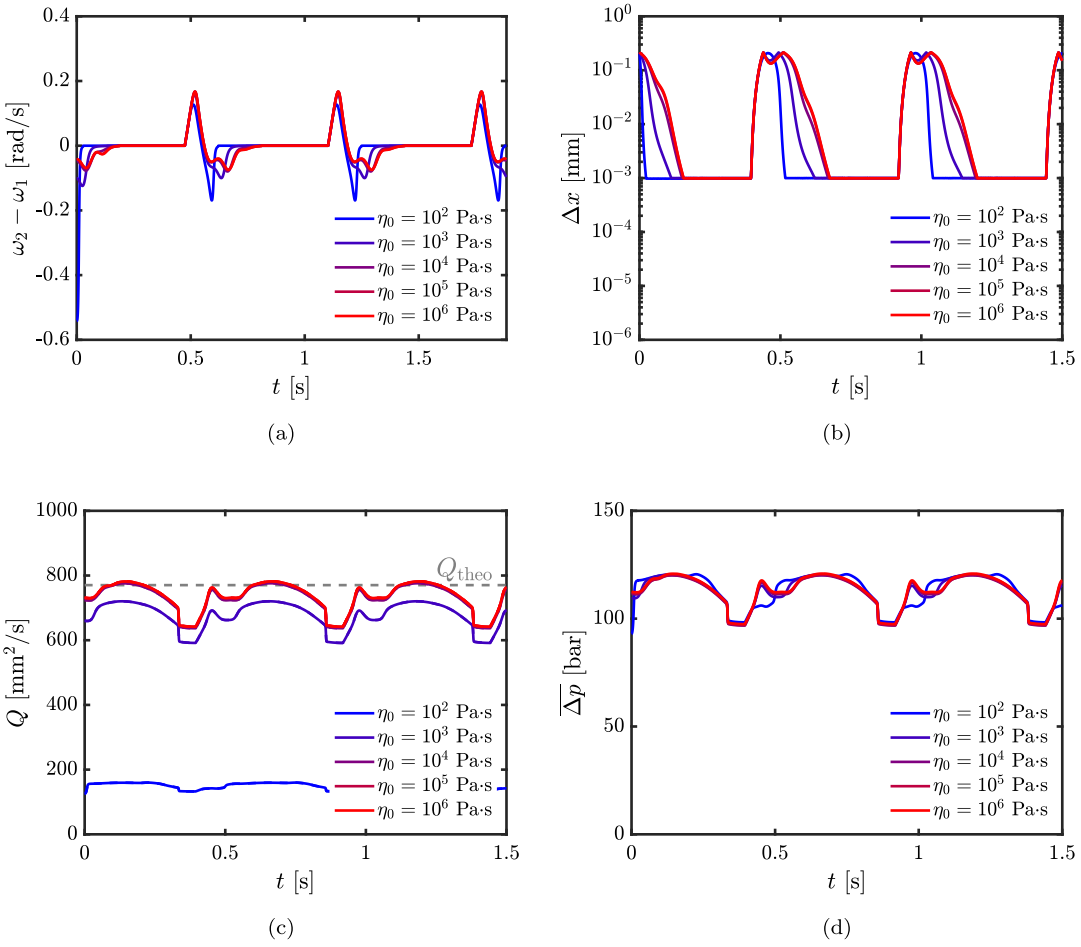

Fig. 6. The output of numerical simulations of the external gear pump, with $\omega_1 = 1$ rad/s, $\overline{\Delta p} \approx 100$ bar, and $d_{\text{min}} = 10^{-3}$ mm, processing Newtonian fluids ($n = 1$) with varying viscosity: (a) rotation speed difference $\omega_2 - \omega_1$, (b) minimum distance Δx, (c) flow rate Q, and (d) mean pressure difference $\overline{\Delta p}$.

the minimum gap size on the output of the pump for an incompressible Newtonian fluid. When the value of d_{min} is large, the rotation of both gears is continuously imposed. This results in a constant rotation speed, and thus a constant minimum distance. A periodic release of contact is observed when decreasing the value of d_{min}. Some time after the release, contact is formed again. The release of contact occurs when one contact point is starting to release and another starts to form. Due to this periodic release of contact, an extra peak in the flow rate of the pump and the pressure difference over the pump arises. When contact is released, the rotation speed of the lower gear increases, resulting in a rise of the flow rate and therewith an increase of the pressure difference. For this Newtonian fluid, it appears that the difference between the output for a value of d_{min} of 10 μ m and 1 μ m is hardly observable. If we compare these values of d_{min} with the typical roughness of the gears [18,19], then 1 μm is quite realistic. This value for the minimum distance is used in all upcoming simulations.

4.3. Viscosity

In our previous work [4] we showed that the output in terms of flow rate and mean pressure difference is determined by the value of the Hersey number:

$$\text{He} = \frac{\eta(\dot{\gamma}_{\text{eff}})\omega_1}{\overline{\Delta p}}. \tag{39}$$

In this work, the Hersey number is varied by changing the viscosity of the fluid. The effect of changing the fluid viscosity on the output is shown in Fig. 6 for an incompressible Newtonian fluid. When decreasing the viscosity the flow rate of the pump decreases due to backflow of the fluid through the clearances, and only when the efficiency of the pump drops, a significant difference in the periods of contact is observed. A lower viscosity then results in a longer period of contact during the rotation of a tooth. For the lowest viscosity, the extra peak in the flow-rate and the pressure-difference fluctuation also disappears.

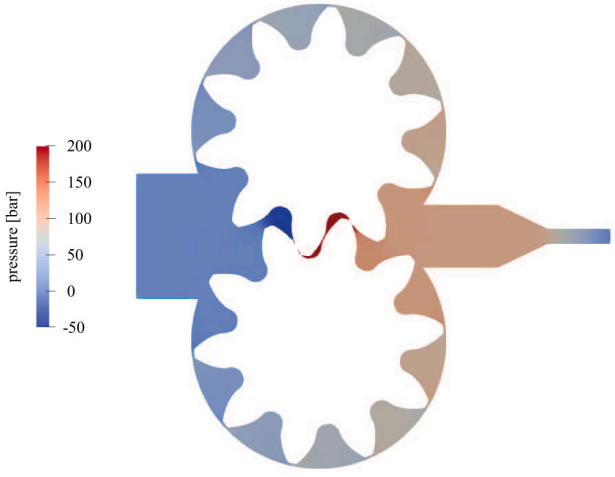

Fig. 7. The pressure distribution in the external gear pump, with $\omega_1 = 1$ rad/s, $\overline{\Delta p} \approx 100$ bar, and $d_{\text{min}} = 10^{-3}$ mm, processing a Newtonian fluid ($n = 1$) with $\eta_0 = 10^4$ Pa s.

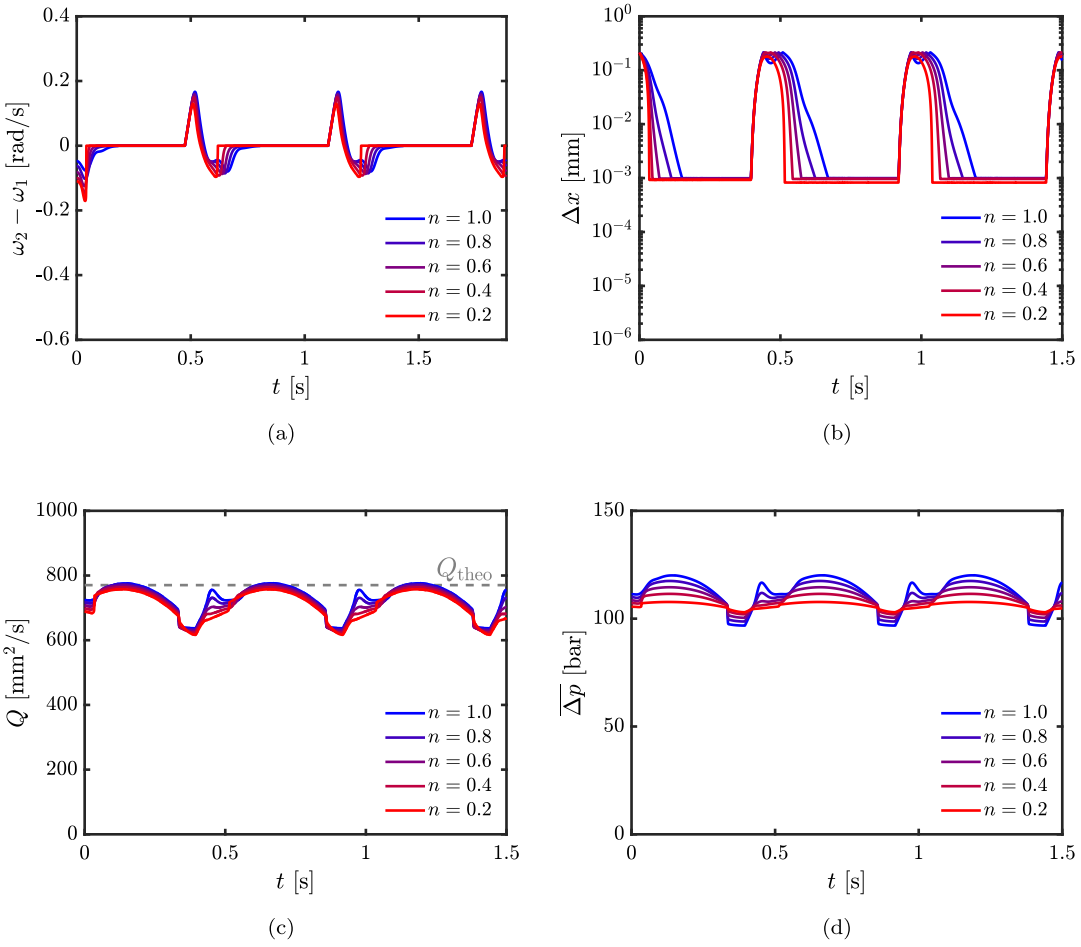

Fig. 8. The output of numerical simulations of the external gear pump, with $\omega_1 = 1$ rad/s, $\overline{\Delta p} \approx 100$ bar, and $d_{\min} = 10^{-3}$ mm, processing shear-thinning fluids with $\eta(\dot{\gamma}_{\text{eff}}) = 10^4$ Pa s and $\lambda = 10$ s, for varying power-law index: (a) rotation speed difference $\omega_2 - \omega_1$, (b) minimum distance Δx, (c) flow rate Q, and (d) mean pressure difference $\overline{\Delta p}$.

The spatial distribution of the pressure for the situation where one contact point is forming and another is releasing, can be seen in Fig. 7 for $\eta_0 = 10^4$ Pa·s. The pressure values observed in the major part of the domain are in a realistic range. However, the maximum pressure that is observed between the gears, i.e. $\max(p) = 6.87 \cdot 10^9$ bar, rises to unrealistic values, which is due to the too limited rheological description of the fluid. These extreme pressures result in the release of contact for a certain period of time. A decrease of the viscosity results in lower pressures between the gears, which consecutively lowers the torque exerted by the fluid on the gears. As a result, the obtained rotation speed of the bottom gear is lower. It is unclear if the change in the formation and release of contact can be fully attributed to the lower pressures as a result of the lower viscosity. Perhaps the drop of the efficiency of the pump also plays an important role. The next step is to add more physics to the rheological model.

4.4. Shear-rate dependence

To investigate the effect of shear-thinning behavior on the output of the external gear pump, the power-law index n in the Carreau model is varied. The results for different power law indices are shown in Fig. 8. As observed in our previous work [4], increasing the amount of shear thinning results in a decrease of the amplitude of the pressure-difference fluctuation. For this reason, the extra peak in the pressure-difference fluctuation also seems to disappear when decreasing the value of n. Interestingly, the amplitude of the extra peak in the flow-rate fluctuation vanishes along with that. Possibly, this is partly resulting from the longer period of contact during the rotation of a gear tooth for increasing amount of shear-thinning behavior.

Also for the shear-thinning fluids, the pressure values in the largest part of the domain are in a realistic range. However, again the maximum pressure observed between the gears is significantly higher. The maximum pressure decreases with increasing amount of shear thinning, i.e. $\max(p) = 1.91 \cdot 10^7$ bar for $n = 0.6$ and $\max(p) = 5.99 \cdot 10^4$ bar for $n = 0.2$. Its value remains however significantly high, although it is much lower than the Newtonian model case. The decrease in maximum pressure can be attributed to the lower viscosity between the gears for shear-thinning fluids as a results of the high shear rates. The lower pressures between the gears result in a shorter period without contact.

4.5. Compressibility

Since locally high pressures are observed in the finite element simulations of the external gear pump, compressibility could play a significant role. Therefore, simulations including compressibility are performed for a strongly shear-thinning fluid. In Table 4, some typical values of the bulk modulus K for different materials are given. Three values of the bulk modulus are considered, i.e. $K = 1$, 10 and 100 GPa.

The results of the compressible simulations are shown in Fig. 9. The introduction of compressibility, results in the simulations having some start-up time before steady state is reached. The lowest bulk modulus results in the longest time to reach a steady-state situation. The start-up times for all simulations remain below the time to rotate the upper gear one gear tooth, since we chose a contraction flow as resistance channel behind the pump to limit the length of the flow problem. For these compressible fluids, the period of contact during the rotation of a gear tooth increases when decreasing the value of the bulk

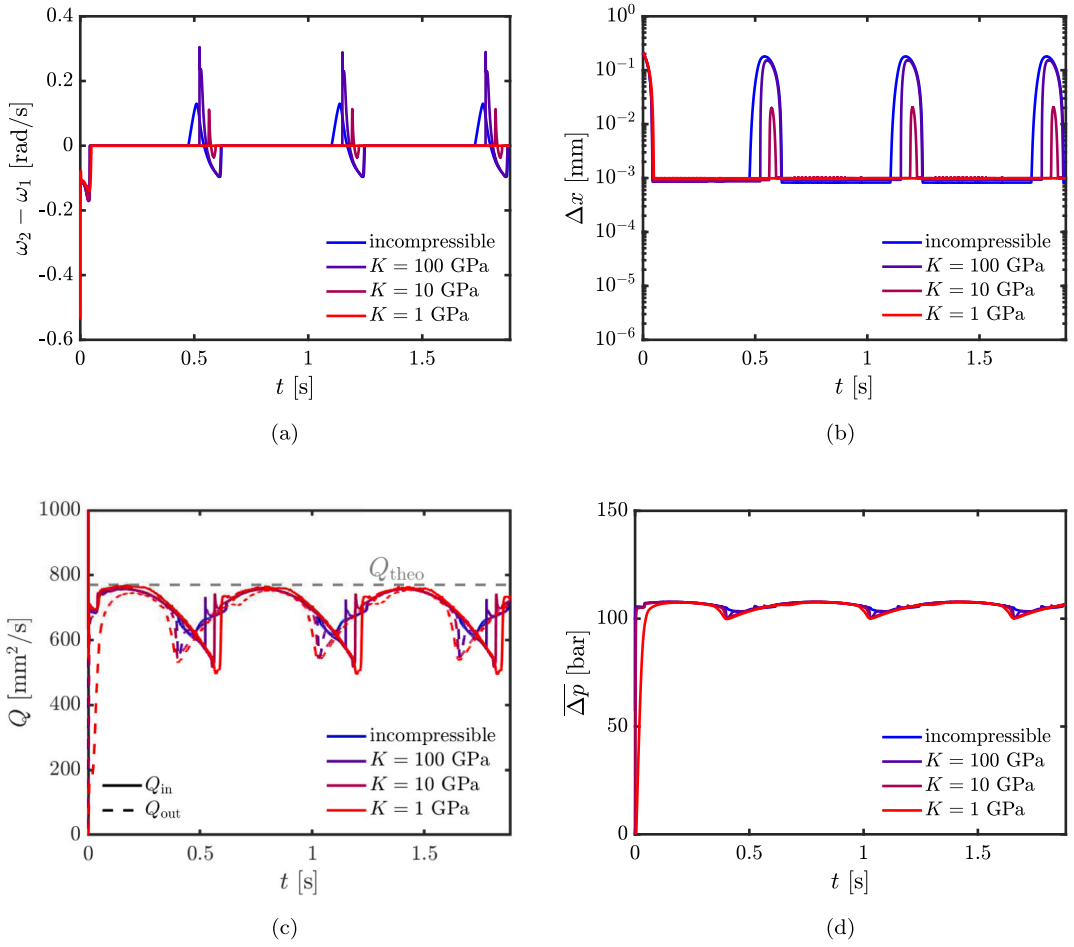

Fig. 9. The output of numerical simulations of the external gear pump, with $\omega_1 = 1$ rad/s, $\overline{\Delta p} \approx 100$ bar, and $d_{\text{min}} = 10^{-3}$ mm, processing compressible shear-thinning fluids with $\eta(\dot{\gamma}_{\text{eff}}) = 10^4$ Pa s, $\lambda = 10$ s and $n = 0.2$, for varying bulk modulus: (a) rotation speed difference $\omega_2 - \omega_1$, (b) minimum distance Δx, (c) flow rate Q, and (d) mean pressure difference $\overline{\Delta p}$.

Table 4
The bulk modulus of some well-known materials [20–23].

Material	K [GPa]
Oil	1.3–3.0
Rubber	2.0–2.5
Water	2.1
Glass	30–100

modulus K. For the lowest value of K, and thus the most compressible fluid, no release of contact is observed at all. The material properties for this strongly compressible and strongly shear-thinning fluid mostly resemble the material behavior of a rubber.

The minimum value of the flow rate at the entry Q_{in} also becomes lower with increasing compressibility. Probably, this is caused by a strong compression of the material at this point in time, instead of the material being pushed out of the pump. The plot of the flow rate shows that for a compressible fluid at a certain point in time, the amount of inflowing material is larger as the amount outflowing material. This means that the fluid must be compressed in order to keep the volume of the problem constant. A small period later, the amount of outflowing material rises above the inflowing material and thus the amount of compression of the material decreases again.

The fluid between the gears is probably strongly compressed when one contact point starts to release and another starts to form. Fig. 10 shows the distribution of the pressure and the relative volume change for the strongly compressible strongly shear-thinning fluid at this point in time, where the relative change in volume is defined as

$$J = \exp\left(-\frac{p - p_{\text{ref}}}{K_{\text{bulk}}}\right). \tag{40}$$

By introducing compressibility, the maximum pressure decreased significantly. Its value is however still considerably large. Between the gears the volume of the fluid is in the order of 65–75% of its volume at the reference pressure. This confirms our hypothesis that the fluid is strongly compressed, instead of being pushed out of the pump.

4.6. Pressure dependence

Since high pressures are observed in the simulations, the influences that pressure can have on the material properties need to be taken into account. Besides compressibility, the viscosity of a fluid can also depend on pressure. An increase in pressure then results in a higher viscosity. As mentioned before, the strongly compressible strongly shear-thinning fluid mostly resembles certain rubbers. For polymers, it is known that they typically have a pressure dependence with β in the order of 1–10 GPa^{-1} [11,12].

The resulting output for different values of the pressure coefficient β is shown in Fig. 11 for the strongly compressible strongly shear-thinning fluid of the previous section. An increasing value of β results in a shorter period of contact during the rotation of a gear tooth. An increasing value of the pressure coefficient also results in a slight increase of the pressure difference over the pump. The flow rate of the pump does not seem to be affected by the pressure dependence of the

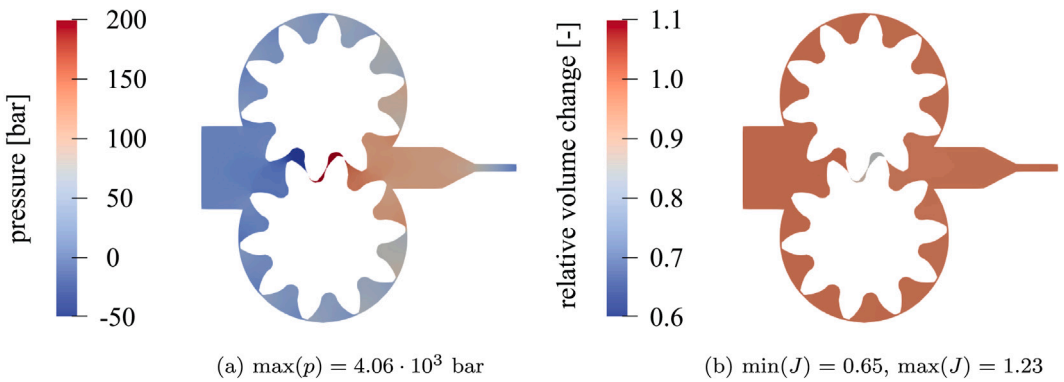

Fig. 10. The distributions of the pressure and the relative volume change in the external gear pump, with $\omega_1 = 1$ rad/s, $\overline{\Delta p} \approx 100$ bar, and $d_{\min} = 10^{-3}$ mm, processing a strongly compressible strongly shear-thinning fluid with $\eta(\dot{\gamma}_{\text{eff}}) = 10^4$ Pa s, $n = 0.2$, $\lambda = 10$ s and $K_{\text{bulk}} = 1$ GPa: (a) pressure p, and (b) relative volume change J.

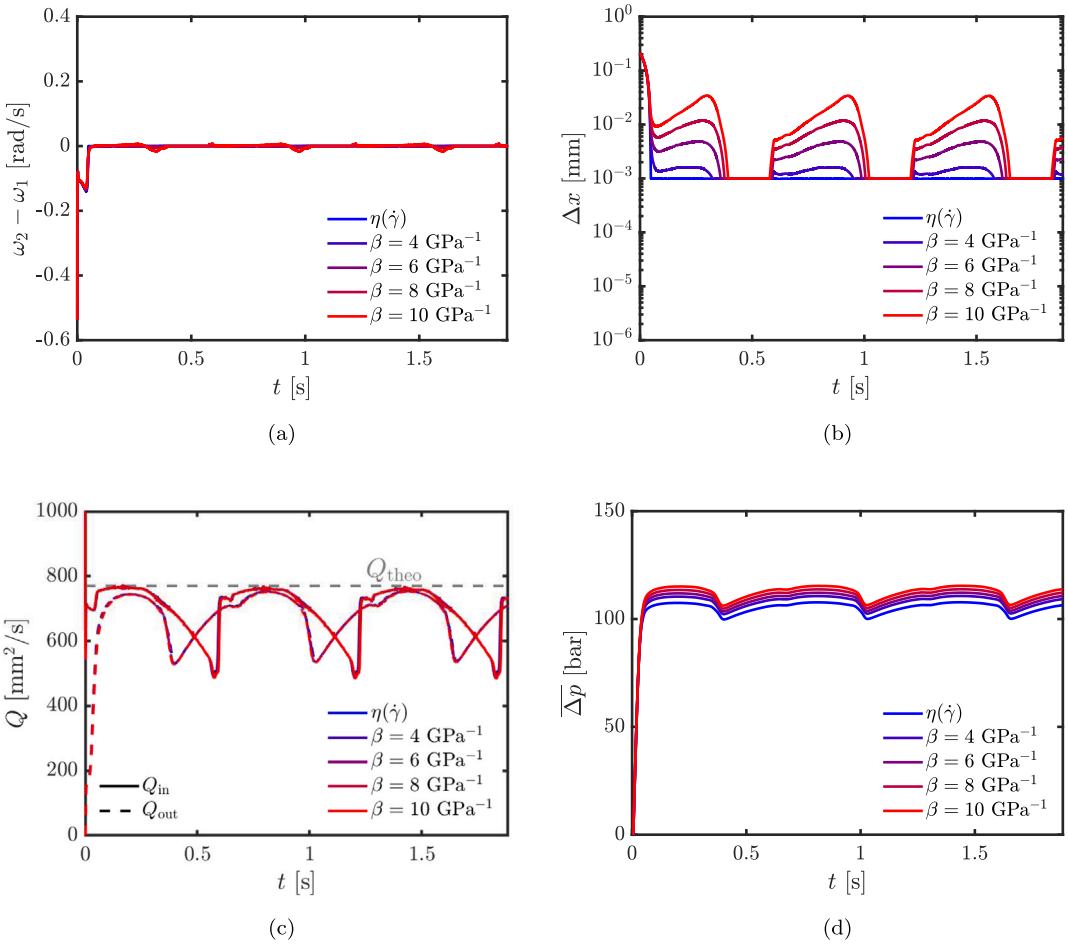

Fig. 11. The output of numerical simulations of the external gear pump, with $\omega_1 = 1$ rad/s, $\overline{\Delta p} \approx 100$ bar, and $d_{\min} = 10^{-3}$ mm, processing compressible shear-thinning fluids that have a pressure-dependent zero-shear viscosity with $\eta(\dot{\gamma}_{\text{eff}}, p_{\text{ref}}) = 10^4$ Pa s, $p_{\text{ref}} = 0$ Pa, $\lambda = 10$ s, $n = 0.2$, $K = 1$ GPa and $\eta_{0,\infty} = 10^2 \eta_{0,\text{ref}}$, for varying pressure coefficient: (a) rotation speed difference $\omega_2 - \omega_1$, (b) minimum distance Δx, (c) flow rate Q, and (d) mean pressure difference $\overline{\Delta p}$.

viscosity. Thus, the pressure dependence of the viscosity mainly locally influences the flow in the external gear pump.

Fig. 12 shows the distribution of the pressure and the viscosity for the $\beta = 10$ GPa^{-1} at the point in time that one contact point forms and another releases. The maximum pressure now increased quite significantly by including a pressure-dependent viscosity. The maximum pressure increased as a result of the local rise in viscosity between the gears with η_0 being in the range of $\eta_{0,\infty}$. The increased pressure between the gears causes the observed release of contact for a certain period of time.

For now, it appears that for a fluid with shear-thinning behavior, compressibility or a pressure-dependent viscosity, contact cannot be prevented during the whole rotation of the gears. Possibly, the normal stresses present in viscoelastic fluids could drive the formation of a lubrication layer between the gears. We did however find that for a strongly shear-thinning strongly compressible fluid, contact can be

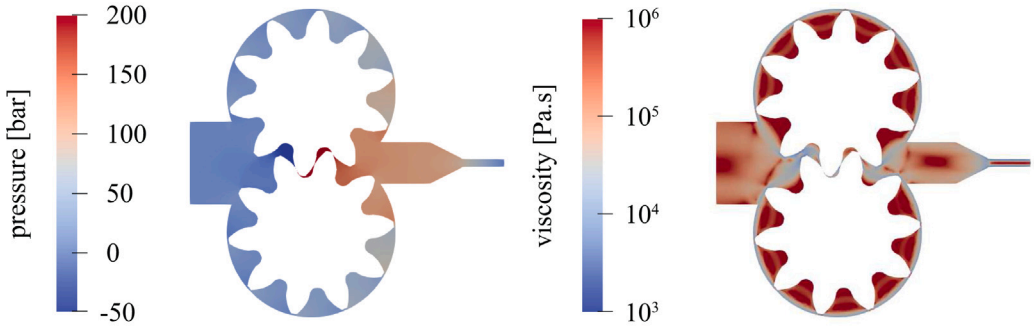

Fig. 12. The distributions of the pressure and the viscosity in the external gear pump, with $\omega_1 = 1$ rad/s, $\overline{\Delta p} \approx 100$ bar, and $d_{\min} = 10^{-3}$ mm, processing a strongly compressible strongly shear-thinning pressure-thickening fluid with $\eta(\dot{\gamma}_{\text{eff}}, p_{\text{ref}}) = 10^4$ Pa s, $p_{\text{ref}} = 0$ Pa, $n = 0.2$, $\lambda = 10$ s, $K_{\text{bulk}} = 1$ GPa, $\eta_{0,\infty} = 10^2 \eta_{0,\text{ref}}$ and $\beta = 10$ GPa^{-1}: (a) pressure p, and (b) viscosity η.

assumed during the full rotation of the gears. Including a pressure-dependent viscosity again results in a release of contact. However, the quite frequently observed temperature dependence of the material properties or the friction that is present in the bearings of the gears could counterbalance this release of contact in reality.

5. Conclusions

In this work, 2D finite element simulations of an external gear pump processing high-viscosity fluids are used to study the formation and release of contact. The gap between the gears becomes quite small with respect to the geometry of the pump. Therefore, meshes are generated using local mesh refinement. The rotation of the upper gear is imposed, whereas the bottom one is freely rotating. To keep the simulations computationally feasible, the minimum distance between the gears is limited to a value $d_{\min}$. If this value is reached, contact is assumed, and thus also the rotation of the bottom gear is imposed. When the rotation of both gears is imposed and the torque on the bottom gear changes sign, which means that the gears want to separate again, contact is released.

With the help of the mass and momentum balance, the velocity and pressure distribution are obtained, but also the rotation speed of the bottom gear. The effect of material properties on the output is studied, where the output is considered in terms of the difference in rotation speed between the gears, minimum distance between the gears, flow rate of the pump, and pressure difference over the pump. When using different values of $d_{\min}$, it was observed that for a Newtonian fluid contact formation is always occurring for the range of values considered. Interestingly, during the rotation of a gear tooth contact is also released for a certain period of time. An extra peak appeared in the flow-rate and pressure-difference fluctuation, exactly at the point in time where contact is released.

For a Newtonian fluid, decreasing the viscosity only resulted in a significantly longer period of contact during the rotation of one gear tooth when the efficiency of the pump dropped. In the flow-rate and pressure-difference fluctuations, the extra peak solely disappeared for the lowest viscosity considered. When shear thinning was introduced, the period of contact during the rotation of a gear tooth increased. Moreover, the amplitude of the pressure-difference fluctuation, including the extra peak, decreased with increasing amount of shear thinning. Also the extra peak in the flow-rate fluctuation lowered for shear-thinning fluids. Thus, for our pump geometry a Newtonian fluid or a fluid with solely a shear-rate dependence always results in the formation and release of contact during the rotation of a gear tooth.

The pressures in the external gear pump, especially locally between the gears, become extremely high. Therefore, the effect of pressure on the material properties is considered. This can be done in two ways; compressibility or a pressure dependence of the viscosity. First, the effect of compressibility was studied for a shear-thinning fluid. The amount of compressibility is varied in the simulations using the bulk modulus. Decreasing the value of the bulk modulus, i.e. increasing compressibility, resulted in longer periods of contact between the contact releases. The release of contact was even prevented when decreasing the value of the bulk modulus to the range of rubbers. Moreover, strong compression of the fluid was observed when including compressibility in the simulations. Including the pressure dependence of the viscosity seems to have the opposite effect. An increasing value of the pressure coefficient results in shorter periods of contact between the contact releases.

It appeared that for a viscous fluid, the formation of contact between the gears in an external gear pump is inevitable. However, for certain fluids the release of contact can be prevented during the whole rotation of a gear. Note that other effects, like a temperature dependence of the fluid properties or viscoelasticity, could also influence the formation and release of contact between the gears of the external gear pump. Furthermore, the assumption of a freely rotating gear could be adapted to a more realistic situation, such as taking into account that there is friction when rotating the gear shaft. In future work, we will however first look at the output predictions of the numerical simulations with respect to extrusion experiments of a polymer melt.

Declaration of competing interest

The authors declare that they have no known competing financial interests or personal relationships that could have appeared to influence the work reported in this paper.

Acknowledgments

The results of this study have been obtained through the FLEX-Pro project (PROJ-00679), which was in part funded by the European Funding for Regional Development (EFRO). The research is performed in collaboration with VMI Holland B.V.

Patrick Anderson reports financial support was provided by VMI.

References

[1] W. Strasser, CFD investigation of gear pump mixing using deforming/agglomerating mesh, J. Fluids Eng. 129 (4) (2007) 476–484.
[2] E. Frosina, A. Senatore, D. Buono, K.A. Stelson, A modeling approach to study the fluid-dynamic forces acting on the spool of a flow control valve, J. Fluids Eng. 139 (1) (2017) 011103.
[3] F. Sedri, A. Riasi, Investigation of leakage within an external gear pump with decompression slots: numerical and experimental study, J. Braz. Soc. Mech. Sci. Eng. 41 (224) (2019).
[4] V.G. de Bie, M.A. Hulsen, P.D. Anderson, Finite element modeling of a viscous fluid flowing through an external gear pump, Macromol. Theory Simul. 30 (1) (2021) 2000060.

[5] D. del Campo, R. Castilla, G.A. Raush, P.J.G. Montero, E. Codina, Numerical analysis of external gear pumps including cavitation, J. Fluids Eng. 134 (8) (2012).
[6] R. Castilla, P.J. Gamez-Montero, D. del Campo, G. Raush, M. Garcia-Vilchez, E. Codina, Three-dimensional numerical simulation of an external gear pump with decompression slot and meshing contact point, J. Fluids Eng. 137 (4) (2015) 041105.
[7] V.G. de Bie, L.S.D.P. Luijten, M.A. Hulsen, P.D. Anderson, Three-dimensional finite element modeling of a viscous fluid flowing through an external gear pump, Macromol. Theory Simul. 2100046 (2021).
[8] M.M.A. Spanjaards, M.A. Hulsen, P.D. Anderson, Die shape optimization for extrudate swell using feedback control, J. Non-Newton. Fluid Mech. 293 (2021) 104552.
[9] M.M.A. Spanjaards, G. Peters, M.A. Hulsen, P.D. Anderson, Numerical study of the effect of thixotropy on extrudate swell, Polymers 13 (24) (2021) 4383.
[10] M.M.A. Spanjaards, G. Peters, M.A. Hulsen, P.D. Anderson, Towards the development of a strategy to characterize and model the rheological behavior of filled, uncured rubber compounds, Polymers (ISSN: 2073-4360) 13 (23) (2021) http://dx.doi.org/10.3390/polym13234068.
[11] R. Cardinaels, P. van Puyvelde, P. Moldenaers, Evaluation and comparison of routes to obtain pressure coefficients from high-capillary rheometry data, Rheol. Acta 46 (4) (2007) 495–505.
[12] H.S. Laun, Pressure dependent viscosity and dissipative heating in capillary rheometry of polymer melts, Rheol. Acta 42 (4) (2003) 295–308.
[13] C. Mitrias, T.R.N. Egelmeers, N.O. Jaensson, M.A. Hulsen, P.D. Anderson, Simulation of bubble growth during the foaming process and mechanics of the solid foam, Rheol. Acta 58 (2019) 131–144.
[14] C. Geuzaine, J.F. Remacle, Gmsh: A 3-D finite element mesh generator with built-in pre- and post-processing facilities, J. Numer. Methods Eng. 79 (2009) 1309–1331.
[15] H.H. Hu, N.A. Patankar, M.Y. Zhu, Direct numerical simulations of fluid-solid systems using the arbitrary Lagrangian-Eulerian technique, J. Comput. Phys. 169 (2) (2001) 427–462.
[16] M. Reberol, C. Georgiadis, J.F. Remacle, Quasi-structured quadrilateral meshin in Gmsh – A robust pipeline for complex CAD models, 2021, arXiv preprint arXiv 2103.04652.
[17] A. Karagiannis, H. Mavridis, A.N. Hrymak, J. Vlachopoulos, A finite element convergence study for shear-thinning flow problems, Internat. J. Numer. Methods Fluids 8 (1988) 123–138.
[18] P. Antoniak, J. Stryczek, Visualization study of the flow processes and phenomena in the external gear pump, Arch. Civ. Mech. Eng. 18 (2018) 1103–1115.
[19] D. Thiagarajan, A. Bratto, A. Vacca, Influence of surface roughness effects on the lubrication performance of external gear machines, in: Proceedings of the ASME/BATH 2017 Symposium on Fluid Power and Motion Control, Vol. FPMC2017-4309, 2017, V001T01A054.
[20] K.S. Varde, Bulk modulus of vegetable oil-diesel fuel blends, Fuel 63 (5) (1984) 713–715.
[21] Y. Jinghong, C. Zhaoneng, L. Yuanzhang, The variation of oil effective bulk modulus with pressure in hydraulic systems, J. Dyn. Syst. Meas. Control 116 (1) (1994) 146–150.
[22] B. Davies, Natural rubber - its engineering characteristics, Mater. Des. 7 (2) (1986) 68–74.
[23] A. Makishima, J.D. Mackenzie, Calculation of bulk modulus, shear modulus and Poisson's ratio of glass, J. Non-Cryst. Solids 17 (1975) 147–157.